Quasi-Free-Standing Epitaxial Graphene on SiC (0001) by Fluorine Intercalation from a Molecular Source

Swee Liang Wong,[†,‡] Han Huang,[‡] Yuzhan Wang,[‡] Liang Cao,[‡,⊥] Dongchen Qi,[‡] Iman Santoso,[§] Wei Chen,[†,‡,§] and Andrew Thye Shen Wee[†,‡,*]

[†]NUS Graduate School for Integrative Sciences and Engineering, National University of Singapore, 28 Medical Drive S117456, Singapore, [‡]Department of Physics, National University of Singapore, 2 Science Drive 3 S117542, Singapore, [§]Department of Chemistry, National University of Singapore, 3 Science Drive 3 S117543, Singapore, and [⊥]National Synchrotron Radiation Laboratory, School of Nuclear Science and Technology, University of Science and Technology of China, Hefei, Anhui 230029, People's Republic of China

ABSTRACT We demonstrated a novel method to obtain charge neutral quasi-free-standing graphene on SiC (0001) from the buffer layer using fluorine from a molecular source, fluorinated fullerene ($C_{60}F_{48}$). The intercalated product is stable under ambient conditions and resistant to elevated temperatures of up to 1200 °C. Scanning tunneling microscopy and spectroscopy measurements are performed for the first time on such quasi-free-standing graphene to elucidate changes in the electronic and structural properties of both the graphene and interfacial layer. Novel structures due to a highly localized perturbation caused by the presence of adsorbed fluorine were produced in the intercalation process and investigated. Photoemission spectroscopy is used to confirm these electronic and structural changes.

KEYWORDS: quasi-free-standing graphene · silicon carbide · fluorine intercalation · scanning tunneling microscopy and spectroscopy · electronic structure · nanostructures

Graphene, a monatomic layer of carbon, has attracted much attention in recent years due to its impressive electronic, optical, mechanical, and thermal properties.[1−4] There are several methods used in the fabrication of graphene, such as mechanical exfoliation, chemical vapor deposition, and chemical reduction of graphene oxides.[5] In particular, those grown on hexagonal SiC (0001) wafers provide a means for integration in existing device technology.[6−10] However, there exist limitations in the usage of such wafers due to the high intrinsic electron doping ($n \approx 10^{13}$ cm^{-2})[7,11] and lower electron mobility (≈2000 cm^2 V^{-1} s^{-1})[10] than that of mechanically exfoliated graphene. This is due to an underlying $6\sqrt{3}\times6\sqrt{3}R30°$ reconstructed interfacial or buffer layer below the graphene layer, which dopes the graphene layer above it and may also provide a source of scattering.[9,12] The buffer layer is made up of honeycomb structures of carbon atoms but has no π-electron dispersion band, as one-third of the carbon atoms are bonded to the Si atoms of the SiC substrate below it.[13−15] The subsequent carbon layer that grows over it does not have interlayer covalent bonds and thus displays the electronic and physical properties of monolayer graphene. For applications in devices, it is thus favorable if the doping level is reduced or the influence of the buffer layer on the overlying graphene is removed.

The intrinsic electron doping can be reduced *via* deposition of p-type dopants such as F4-TCNQ molecules[16,17] or Au atoms.[18] Removal of the underlying buffer layer to reduce its doping contribution and improve electron mobility in the epitaxial graphene layer has been performed using hydrogen, lithium, oxygen, and, most recently, fluorine intercalation, which breaks the Si−C bonds holding the buffer layer, in turn converting it into graphene.[19−22] These intercalated products have been intensively studied using PES and LEEM measurements,[19−22] but scanning tunneling microscopy (STM) experiments have not been carried out to study the effects of intercalation on graphene and the interfacial layer at the nanometer scale. Fluorination of graphene has also been studied intensively both experimentally and theoretically recently.[23−26] Thus, it would be of interest to investigate any occurrence and nature of fluorination of the graphene layer during the intercalation process. In this work, we demonstrated successful fluorine intercalation using the fluorinated fullerene molecule, $C_{60}F_{48}$, as a precursor.[27−29] $C_{60}F_{48}$ was chosen as it is a known fluorinating agent[30,31] and also allows the safe introduction of fluorine. Decoupling of the buffer layer from the substrate and the associated physical and electronic structural changes are observed *via* low-temperature scanning

* Address correspondence to phyweets@nus.edu.sg.

Received for review July 31, 2011 and accepted August 27, 2011.

Published online August 27, 2011
10.1021/nn202910t

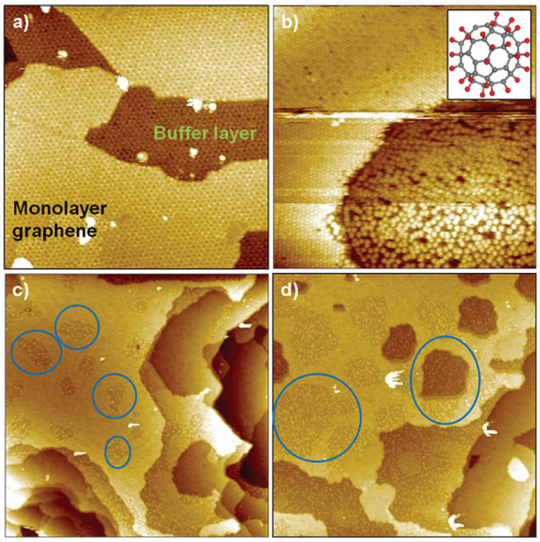

Figure 1. (a) 100 nm × 100 nm STM image of a surface having both a buffer layer and graphene monolayer prior to deposition (V_{tip} = 2.0 V, I = 100 pA). (b) 80 nm × 80 nm STM image of surface, (left) graphene and (right) buffer layer, covered by $C_{60}F_{48}$ (V_{tip} = −3.0 V, I = 100 pA). Inset: Model of $C_{60}F_{48}$. (c) 200 × 190 nm STM images of surface after applying procedures once. (d) Surface after applying procedure 4 times (both c and d images V_{tip} = −2.0 V, I = 100 pA). Some of the intercalated areas are circled in blue.

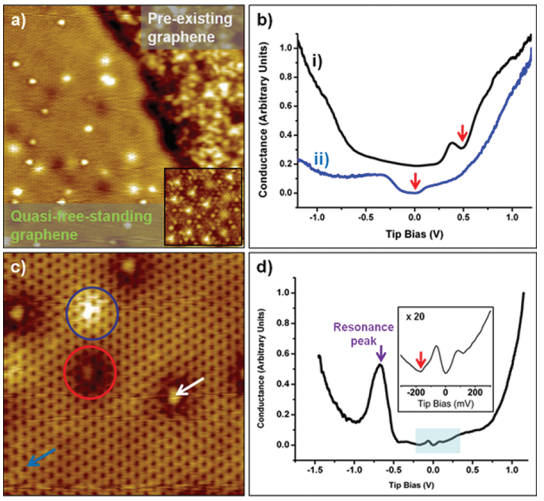

Figure 2. (a) 20 nm × 20 nm STM image showing intercalation-induced quasi-free-standing graphene monolayer joined continuously with pre-existing graphene monolayer. (V_{tip} = −0.35 V, I = 100 pA). Inset: High-resolution 8 × 8 nm^2 STM image of clean epitaxial graphene with existing underlying buffer layer (V_{tip} = −0.5 V, I = 100 pA). (b) Averaged dI/dV spectra taken on (i) pre-existing graphene and (ii) decoupled graphene at points away from protrusion, an example indicated by a blue arrow in c). (c) 7 nm × 7 nm STM image of surface (V_{tip} = −0.25 V, I = 100 pA). (d) dI/dV spectra taken over protrusions on decoupled graphene, as indicated by a white arrow. (b and d) Red arrows indicate position of Dirac point and purple arrow indicates position of resonance peak.

tunneling microscopy (LT-STM). Novel structures were formed on the decoupled graphene and were attributed to a dilute fluorination of the decoupled graphene. Its influence on the electronic structure was measured using scanning tunneling spectroscopy (STS). Synchrotron radiation based photoemission spectroscopy (PES) confirms both intercalation-induced physical and electronic changes observed under STM/STS.

RESULTS AND DISCUSSION

Figure 1a shows the STM image of the substrate surface containing both buffer and monolayer graphene prior to $C_{60}F_{48}$ deposition. The exposed buffer layer in the center of the image (darker region) is noted to be much rougher than the surrounding area covered with graphene.[32] In Figure 1b, the STM image of the as-deposited $C_{60}F_{48}$ molecules, represented by spherical objects, is shown. The molecules adsorbed on graphene form a closely packed layer, while those on the buffer layer adsorb in a disordered arrangement. The structural contrast between the molecules on separate surfaces implies that the adsorption energy of $C_{60}F_{48}$ on the interfacial layer is higher than those on graphene, thus limiting its diffusion and ability to form a close packed layer. After annealing, intercalation and decoupling of the interfacial layer from the substrate took place. Figure 1c and d are the STM images of the substrate surface after the deposition and annealing procedures were performed once and for four times, respectively. In the regions outlined with blue circles (Figure 1c), the underlying buffer layer was no longer observed under STM (Figure 2a). Hence, we termed these regions, in accordance with prior reports, to be quasi-free-standing graphene.[20] From the observed coverage of quasi-free-standing epitaxial graphene, we note that complete intercalation was not achievable within a single cycle, and it can be increased with subsequent repeats of the procedure. By calculating the decoupled graphene to buffer layer area ratio over STM images covering a total area of about 80 000 nm^2, the ratio is estimated to increase from 0.69 (after one cycle) to 1.87 after repeating the procedure three more times. Throughout the experiment, only the buffer layer was affected and hence converted into monolayer quasi-free-standing graphene. Neither conversion of the pre-existing graphene monolayer into bilayer graphene nor modification of the monolayer graphene was observed. This was verified by repeating the same procedure on monolayer epitaxial graphene on SiC (0001), where no observable effect can be found. This may be related to the weaker method of intercalation employed at a lower temperature of 150 °C that results in fluorine intercalating only under regions where the buffer layer is exposed. This is in contrast with other methods that involve direct application of H_2 and Li intercalants at elevated temperatures.[19−21] The lower adsorption energy of the molecules on the regions of monolayer epitaxial graphene may also limit the extent of fluorine migration from the molecules to

the interface before desorption of the molecule occurs. We note that these intercalated samples and the observed morphology are stable under temperatures of up to 1200 °C, higher than that of other intercalated products.[19,21]

Figure 2a displays the STM image at the boundary between an unperturbed pre-existing graphene monolayer and such a quasi-free-standing graphene layer. By taking a topographical derivative of the image at the boundary (see Figure S1 in the Supporting Information), the two surfaces are observed to be in the same continuous layer. We note that the $6\sqrt{3}\times6\sqrt{3}R30°$ reconstructed buffer layer below the quasi-free-standing graphene was absent as compared to that of the pre-existing graphene layer. An inset showing the buffer layer imaged through epitaxial graphene is presented for comparison. This is a clear indication that fluorine intercalation and the subsequent physical decoupling of the interfacial layer from the substrate have taken place. Apart from the absence of the underlying buffer layer, novel structures due to the intercalation process were also observed. Figure 2c depicts a high-resolution STM image of these structures. These structures consist of circular protrusions with no distinct structure (circled in red) and diffusive bright spots above which the graphene structure is still observed (circled in blue). These diffusive bright spots all have heights < 0.1 nm and are attributed to the undulations of the graphene layer. The height of the circular protrusions with no distinct structure was measured to be 0.04 ± 0.05 nm, much smaller than typical bond lengths, ≥ 0.1 nm. This excludes its origin from intercalated $C_{60}F_{48}$ molecules or its associated molecular fragments left below the layer. Furthermore, the surrounding area of the protrusions does not show any electron-scattering patterns that one would observe about vacancy or point defects of graphene.[33,34] Thus, we propose that these circular protrusions are due to subsurface fluorine atoms bonded to the decoupled graphene. This will be further corroborated later by the observed electronic structural changes. These observed structures may negatively influence the mobility of the as-obtained quasi-free-standing graphene due to an enhanced electronic scattering about them. However, the extent of this degradation is still unclear due to the dilute amounts of these structures (<0.01% of the graphene layer) and also the lack of electronic scattering observed under STM. Transport measurements would be required to ascertain the mobility of this as-obtained quasi-free-standing graphene and is a subject for future work.

In addition to a structural transformation, there is also a significant change in the electronic structure of the decoupled graphene, as shown by STS in Figure 2b and d. Spectra (i) and (ii) in Figure 2b were averaged over 5000 STS spectra taken at random points on the pre-existing monolayer graphene and also at points away from the protrusions on the quasi-free-standing graphene, respectively. Both spectra were taken after the deposition and annealing procedures were carried out. The obtained spectra are characteristic of those performed on 2DEG systems,[33,35−37] with one minimum at the Fermi level and another at the Dirac point. From the STS measurements (spectrum i), the quasi-free-standing graphene has its Dirac point, E_D, at the charge neutrality point; that is, the quasi-free-standing graphene is undoped. This differs from that of the pre-existing monolayer epitaxial graphene (spectrum ii), which has its Dirac point at 500 meV below the Fermi energy, similar to other reports for as-grown monolayer graphene on SiC (0001).[38−41] This confirms the presence of quasi-free-standing-graphene as the electron-doping effect from the buffer layer is removed along with it, having the same effect as those of hydrogen-intercalated ones.[21] The absence of any shift in the Dirac point or additional electronic features in the conductance spectrum (spectrum ii) indicates that there are no observable effects on the pre-existing monolayer graphene after annealing the molecular covered surface. We note that the extent of doping (approximately charge neutral) of our obtained quasi-free-standing graphene is much less than the values (Dirac point at 0.79 eV above Fermi level) reported by Rotenberg *et al.*[22] This is because local STM measurements may not reflect the same level of doping that averaged angular resolved photoemission spectroscopy measurements show. In addition, their work involves a surface consisting of only fluorine-intercalated quasi-free-standing graphene produced using a XeF_2 source. In contrast, the surface of interest in this article consists of a mixture of both pre-existing epitaxial graphene and quasi-free-standing graphene, which results in p-type doping not being observed.

Figure 2d shows the STS performed on the protrusions of the quasi-free-standing graphene. In addition to the expected STS of a graphene monolayer, there is a resonance peak located 600 meV above the Fermi level in the conduction band. Theoretical calculations have shown that such a peak can be induced by a highly localized impurity on graphene, causing a perturbation in the onsite potential energy at its location.[42] The location of the peak in the conduction band indicates that this impurity has an attractive potential. This impurity also induces a slight p doping of the graphene at its location, as the Dirac point is now observed to be at 175 meV above the Fermi level. This is expected, as an attractive impurity potential would draw electrons away from the regions of graphene in its vicinity. In addition, STS measurements performed at points with varying distances from the center of the protrusion (not shown) indicate an almost instant decay of this resonance peak at points beyond the edge of the protrusion, indicating a highly localized potential perturbation that a strongly adsorbed adatom

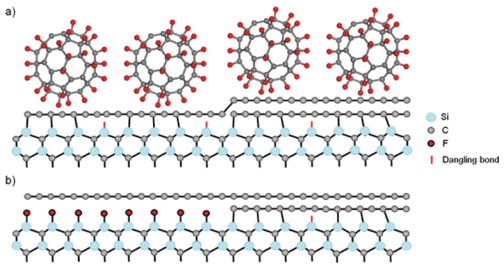

Figure 3. Schematic model describing (a) $C_{60}F_{48}$ molecules deposited on a surface having both monolayer graphene and buffer layer and (b) continuous surface of quasi-free-standing graphene monolayer and nonintercalated monolayer graphene after annealing at temperatures of 150 and 850 °C.

would provide. These STS measurements corroborate our hypothesis that the protrusions are due to electronegative fluorine atoms being bonded to the decoupled graphene from below. Hence, they exert a localized attractive impurity potential that causes the observed electronic structural changes. Deviations with theoretical calculations in terms of peak position is expected, as the model used does not take into account the extent of change from sp^2 to sp^3 hybridization of the C−C bonds after adsorption of fluorine. We note that the appearance of these round protrusions is different from those found in a recent report. In that report, strong 3-fold electronic scattering patterns are observed in the regions of graphene where fluorine is covalently bonded.[43] Rather, the appearance of the protrusions in our STM measurements is similar to a study on graphite where a portion of fluorine atoms was ionically bonded to the graphite surface without forming a significant electronic scattering.[44] This implies that in our studies the fluorine atoms are also ionically bonded to the graphene layer from below and the π-dispersion bands are not completely disrupted. Hence, we put forth a model in Figure 3 that describes the process. After annealing the $C_{60}F_{48}$-covered substrate at 150 °C as depicted in Figure 3a, fluorine migration took place from the molecules to the interfacial layer. Complete molecular desorption and decoupling of the buffer layer then occurred at 800 °C, and the resultant effect is summarized in Figure 3b. The migrating fluorine molecules broke the Si−C bonds between the buffer layer and the substrate, releasing the buffer layer to form quasi-free-standing graphene and forming a passivated Si−F interfacial layer between the two. Additional modifications to the quasi-free-standing graphene occurred in the form of fluorine adsorption from below (not shown in the model of Figure 3b), which created the observed novel physical and electronic structures.

To ascertain the fluorine intercalation, core level PES using synchrotron radiation was carried out. Si 2p, C 1s, and F 1s spectra were measured for the fluorine-intercalated product and also for a monolayer epitaxial

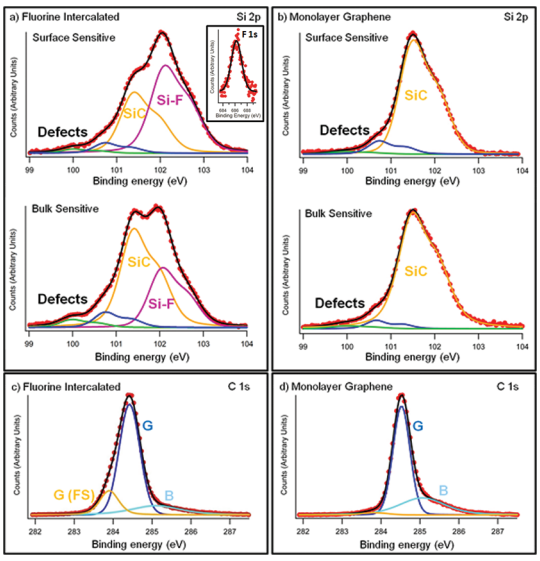

Figure 4. Si 2p core level spectra for (a) fluorine-intercalated graphene sample. Inset: F 1s core level spectra taken with photon energy = 750 eV. (b) Si 2p core level spectra of monolayer graphene. The spectra in the top panel are collected with the beam emission 50° away from surface normal (surface sensitive), while the spectra in the bottom panel are collected with the detector placed at an angle of normal emission (bulk sensitive). Photon energy = 140 eV for the Si 2p spectra. C 1s core level spectra for (c) fluorine-intercalated graphene sample and (d) monolayer graphene. Photon energy = 350 eV with the detector placed at normal emission angles for C 1s spectra. Experimental data are displayed in red dots. The black solid line is the envelope of the fitted components, which are labeled accordingly.

graphene on SiC (0001) for comparison. The F 1s signal was detected for the fluorine-intercalated sample at a binding energy of 686.2 ± 0.1 eV and is shown in the inset of Figure 4a. No apparent asymmetry is noted in the peak shape, and a single peak is used to fit it. Depth position of various species in the substrates is differentiated by changing the angle of electron emission detected from emission normal to the surface (bulk sensitive) and 50° away from surface normal (surface sensitive). Figure 4a and b show the Si 2p spectra for fluorine-intercalated and monolayer epitaxial graphene, respectively. The Si 2p peaks are made up of spin−orbit split doublets, and the binding energies are given with respect to the Si $2p_{3/2}$ position. Both spectra consist of a dominant Si 2p peak at 101.4 ± 0.1 eV due to the bulk SiC component. The slight shoulder at 100.7 ± 0.1 eV is attributed to another bulk component present in the $6\sqrt{3}\times6\sqrt{3}R30°$ area of the SiC(0001) substrate as described by others.[45] For the fluorine-intercalated sample, there is an additional Si 2p component at a higher binding energy of 102.1 ± 0.1 eV due to the Si−F bonds. This is expected, as fluorine has a higher electronegativity than carbon. When a surface-sensitive emission beam angle (50°) is used, the Si 2p peak signal from the Si−F component is stronger than that of bulk SiC. In contrast, when it is taken at normal electron emission angles (bulk sensitive), the Si 2p peak

signal from the Si−F component is weaker than that of bulk SiC. This indicates that the Si−F bond is a near-surface component. This confirms the presence of a fluorine-passivated silicon interfacial layer between the quasi-free-standing graphene layer and the SiC substrate after intercalation, as described by our model in Figure 3b. Another additional smaller component at 100.0 ± 0.1 eV is attributed to the presence of defects possibly in the form of Si clusters after the Si−C bonds were broken during intercalation. There is no observable shift in the bulk SiC component as compared to that of the reference sample, indicating that the band bending induced by the formation of surface Si−F bonds is similar to that of the Si−C bonds in the buffer layer.[15]

Figure 4c and d show the C 1s core level spectra taken using photon energies of 350 eV at normal electron emission for both intercalated and reference samples. Experimental data points are shown as red dots, while the black line is an envelope of the fitted components. For both spectra, the highest peak at 284.4 ± 0.1 eV belongs to that of graphene with an existing underlying buffer layer, while the shoulder situated at a higher binding energy of 285.1 ± 0.1 eV belongs to the buffer layer.[15,16] The difference between spectra is the appearance of a component, labeled G(FS) in Figure 4c, at a lower binding energy of 283.9 ± 0.1 eV in the C 1s spectrum of the intercalated sample. This is attributed to the quasi-free-standing graphene, and the difference of 0.5 eV between the two components agrees perfectly with the difference in Dirac point positions between the pre-existing and quasi-free-standing graphene observed from STS measurements in Figure 2b. Due to the small amount of C−F bonds present (<0.01%), as indicated by the dilute distribution of protrusions in the STM images, they are not detected in the C 1s core level PES.

CONCLUSION

In summary, we have successfully performed fluorine intercalation using a molecular source to form a charge neutral quasi-free-standing graphene layer. The as-formed quasi-free-standing epitaxial graphene was investigated for the first time using STM/STS measurements and would prove useful in understanding other experiments of similar nature. The STM/STS results confirmed the associated physical and electronic changes due to an intercalation process, and these changes were further verified using PES. The intercalation process was highly selective and only took place on the buffer layer due to its weak nature of intercalation. Thus, this allows the formation of a surface consisting only of monolayer epitaxial graphene even if the substrate surface was inhomogeneous and had regions of monolayer graphene prior to intercalation. In addition to the formation of a quasi-free-standing graphene layer, dilute amounts of novel structures that locally alter the electronic structure of graphene were also observed and attributed to fluorine atoms bonded to graphene from below. Such adsorption of adatoms provides the possibility of local tuning of the electronic properties of graphene. The quasi-free-standing graphene remains very stable in ambient atmospheres for up to five months with no change detected under core level PES, STM, and STS measurements. This stability under ambient conditions indicates its robustness for implementation in devices.

METHODS

The substrates used were cut from a commercially available (Cree Inc.) on-axis oriented 4H-SiC (0001) wafer doped with nitrogen (10^{17} cm^{-3}) and prepared by chemical-mechanical polishing. A sample having surfaces containing both epitaxial monolayer graphene and buffer layer in equal coverage was used in the intercalation process. Another 4H-SiC (0001) sample having a monolayer epitaxial graphene was also prepared and measured using PES to act as a reference. Both samples were grown *via* graphitization under ultra-high-vacuum conditions,[7,9,11] and the STM images of the pristine surfaces were first acquired to confirm the surface cleanliness. $C_{60}F_{48}$ (95% purity, Term USA) was first thermally evaporated at 110 °C from a Knudsen cell onto the sample kept at room temperature under ultra-high-vacuum conditions. Deposition was performed at a rate of about 0.05 monolayer/min (as approximated from STM images) to achieve a monolayer of molecules prior to annealing. The sample was checked under LT-STM for purity and quality of the molecular layer. A direct current was then passed through the sample for an initial annealing at approximately 150 °C to allow fluorine migration from the molecule to the interface below the buffer layer. The same method of annealing was then carried out at a higher temperature of 800 °C to complete the decoupling process. LT-STM and STS was used to analyze the morphological and electronic properties of the thus-formed decoupled epitaxial graphene layer, and core level PES was used to verify the structural and electronic changes of the sample after intercalation. *In situ* LT-STM experiments were carried out in a custom-built multichamber ultra-high-vacuum system having a base pressure lower than 1.0×10^{-10} mbar and housing an Omicron LT-STM.[46] STM imaging was carried out at 77 K in constant current mode with a chemically etched tungsten tip. PES measurements are performed at the SINS beamline at the Singapore Synchrotron Light Source.[47,48] Photon energy used for the Si 2p and C 1s spectra are 140 and 350 eV, respectively.

Acknowledgment. The authors acknowledge the support from NRF-CRP grant R-143-000-360-281 "Graphene and Related Materials and Devices" and NUS YIA Grant R143-000-452-101. S.L.W. acknowledges a NUS Graduate School for Integrative Sciences and Engineering Scholarship. The authors also thank V. M. Pereira for the insightful discussion.

Supporting Information Available: STM images showing continuous boundary between quasi-free-standing graphene and monolayer epitaxial graphene. This material is available free of charge via the Internet at http://pubs.acs.org.

REFERENCES AND NOTES

1. Novoselov, K. S.; Geim, A. K.; Morozov, S. V.; Jiang, D.; Katsnelson, M. I.; Grigorieva, I. V.; Dubonos, S. V.; Firsov, A. A. Two-Dimensional Gas of Massless Dirac Fermions in Graphene. *Nature* **2005**, *438*, 197–200.
2. Novoselov, K. S.; Jiang, D.; Schedin, F.; Booth, T. J.; Khotkevich, V. V.; Morozov, S. V.; Geim, A. K. Two-Dimensional Atomic Crystals. *Proc. Natl. Acad. Sci. U. S. A.* **2005**, *102*, 10451–10453.
3. Zhang, Y.; Tan, Y. W.; Stormer, H. L.; Kim, P. Experimental Observation of the Quantum Hall Effect and Berry's Phase in Graphene. *Nature* **2005**, *438*, 201–204.
4. Novoselov, K. S.; Geim, A. K.; Morozov, S. V.; Jiang, D.; Zhang, Y.; Dubonos, S. V.; Grigorieva, I. V.; Firsov, A. A. Electric Field Effect in Atomically Thin Carbon Films. *Science (New York, N.Y.)* **2004**, *306*, 666–669.
5. Geim, A. Graphene: Status and Prospects. *Science* **2009**, *324*, 1530–1534.
6. Berger, C.; Song, Z.; Li, X.; Wu, X.; Brown, N.; Naud, C.; Mayou, D.; Li, T.; Hass, J.; Marchenkov, A. N.; *et al*. Electronic Confinement and Coherence in Patterned Epitaxial Graphene. *Science (New York, N.Y.)* **2006**, *312*, 1191–1196.
7. Ohta, T.; Bostwick, A.; Seyller, T.; Horn, K.; Rotenberg, E. Controlling the Electronic Structure of Bilayer Graphene. *Science (New York, N.Y.)* **2006**, *313*, 951–954.
8. Berger, C.; Wu, X.; First, P.; Conrad, E.; Li, X.; Sprinkle, M.; Hass, J.; Varchon, F.; Magaud, L.; Sadowski, M.; *et al*. Dirac Particles in Epitaxial Graphene Films Grown on SiC. *Adv. Solid State Phys.* **2008**, *47*, 145–145.
9. Riedl, C.; Starke, U. Structural Properties of the Graphene-SiC(0001) Interface As a Key for the Preparation of Homogeneous Large-Terrace Graphene Surfaces. *Phys. Rev. B* **2007**, *76*, 245406.
10. Emtsev, K. V.; Bostwick, A.; Horn, K.; Jobst, J.; Kellogg, G. L.; Ley, L.; McChesney, J. L.; Ohta, T.; Reshanov, S. A.; Röhrl; *et al*. Towards Wafer-Size Graphene Layers by Atmospheric Pressure Graphitization of Silicon Carbide. *Nat. Mater.* **2009**, *8*, 203–207.
11. Riedl, C.; Zakharov, A. A.; Starke, U. Precise *In Situ* Thickness Analysis of Epitaxial Graphene Layers on SiC(0001) Using Low-Energy Electron Diffraction and Angle Resolved Ultraviolet Photoelectron Spectroscopy. *Appl. Phys. Lett.* **2008**, *93*, 033106.
12. Mallet, P.; Varchon, F.; Naud, C.; Magaud, L.; Berger, C.; Veuillen, J. Y. Electron States of Mono- and Bilayer Graphene on SiC Probed by Scanning-Tunneling Microscopy. *Phys. Rev. B* **2007**, *76*, 041403(R).
13. Emtsev, K. V.; Speck, F.; Seyller, T.; Ley, L. Interaction, Growth, and Ordering of Epitaxial Graphene on SiC{0001} Surfaces: A Comparative Photoelectron Spectroscopy Study. *Phys. Rev. B* **2008**, *77*, 155303.
14. Mattausch, A.; Pankratov, O. Ab Initio Study of Graphene on SiC. *Phys. Rev. Lett.* **2007**, *99*, 076802.
15. Bostwick, A.; Emtsev, K.; Horn, K.; Huwald, E.; Ley, L.; McChesney, J.; Ohta, T.; Riley, J.; Rotenberg, E.; Speck, F.; *et al*. Photoemission Studies of Graphene on SiC: Growth, Interface, and Electronic Structure. *Adv. Solid State Phys.* **2008**, *47*, 159–170.
16. Chen, W.; Chen, S.; Qi, D. C.; Gao, X. Y.; Wee, A. T. S. Surface Transfer P-Type Doping of Epitaxial Graphene. *J. Am. Chem. Soc.* **2007**, *129*, 10418–10422.
17. Coletti, C.; Riedl, C.; Lee, D. S.; Krauss, B.; Patthey, L.; von Klitzing, K.; Smet, J. H.; Starke, U. Charge Neutrality and Band-Gap Tuning of Epitaxial Graphene on SiC by Molecular Doping. *Phys. Rev. B* **2010**, *81*, 235401.
18. Gierz, I.; Suzuki, T.; Weitz, R. T.; Lee, D. S.; Krauss, B.; Riedl, C.; Starke, U.; Höchst, H.; Smet, J. H.; Ast, C. R.; *et al*. Electronic Decoupling of an Epitaxial Graphene Monolayer by Gold Intercalation. *Phys. Rev. B* **2010**, *81*, 235408.
19. Virojanadara, C.; Watcharinyanon, S.; Zakharov, A.; Johansson, L. Epitaxial Graphene on 6H-SiC and Li Intercalation. *Phys. Rev. B* **2010**, *82*, 205402.
20. Oida, S.; McFeely, F.; Hannon, J.; Tromp, R.; Copel, M.; Chen, Z.; Sun, Y.; Farmer, D.; Yurkas, J. Decoupling Graphene From SiC(0001) *via* Oxidation. *Phys. Rev. B* **2010**, *82*, 041411(R).
21. Riedl, C.; Coletti, C.; Iwasaki, T.; Zakharov, A. A.; Starke, U. Quasi-Free-Standing Epitaxial Graphene on SiC Obtained by Hydrogen Intercalation. *Phys. Rev. Lett.* **2009**, *103*, 246804.
22. Walter, A. L.; Jeon, K. J.; Bostwick, A.; Speck, F.; Ostler, M.; Seyller, T.; Moreschini, L.; Kim, Y. S.; Chang, Y. J.; Horn, K.; *et al*. Highly P-Doped Epitaxial Graphene Obtained by Fluorine Intercalation. *Appl. Phys. Lett.* **2011**, *98*, 184102.
23. Şahin, H.; Topsakal, M.; Ciraci, S. Structures of Fluorinated Graphene and Their Signatures. *Phys. Rev. B* **2011**, *83*, 11532.
24. Jeon, K. J.; Lee, Z.; Pollak, E.; Moreschini, L.; Bostwick, A.; Park, C. M.; Mendelsberg, R.; Radmilovic, V.; Kostecki, R.; Richardson, T. J.; *et al*. Fluorographene: A Wide Bandgap Semiconductor with Ultraviolet Luminescence. *ACS Nano* **2011**, *5*, 1042–1046.
25. Samarakoon, D. K.; Chen, Z.; Nicolas, C.; Wang, X. Q. Structural and Electronic Properties of Fluorographene. *Small* **2011**, *7*, 965–969.
26. Nair, R. R.; Ren, W.; Jalil, R.; Riaz, I.; Kravets, V. G.; Britnell, L.; Blake, P.; Schedin, F.; Mayorov, A. S.; Yuan, S.; *et al*. Fluorographene: A Two-Dimensional Counterpart of Teflon. *Small* **2010**, *6*, 2877–2884.
27. Bulusheva, L. G.; Okotrub, A. V.; Boltalina, O. V. Electronic Structure of the Fluorinated Fullerene $C_{60}F_{48}$. *J. Phys. Chem. A* **1999**, *103*, 9921–9924.
28. Troyanov, S.; Troshin, P.; Boltalina, O.; Ioffe, I.; Sidorov, L.; Kemnitz, E. Two Isomers of $C_{60}F_{48}$: An Indented Fullerene. *Angew. Chem., Int. Ed.* **2001**, *40*, 2285–2287.
29. Kniaz, K.; Fischer, J.; Selig, H.; Vaughan, G.; Romanow, W.; Cox, D.; Chowdhury, S.; McCauley, J.; Strongin, R.; Smith, A., III. Fluorinated Fullerenes: Synthesis, Structure, and Properties. *J. Am. Chem. Soc.* **1993**, *115*, 6060–6064.
30. Sadowski, J.; Fujikawa, Y.; Kelly, K.; Nakayama, K.; Sakurai, T.; Mickelson, E.; Hauge, R.; Margrave, J. Fluorinated Fullerene Thin Films Grown on the Si (1 1 1)-7×7 Surfaces--STM and HREELS Investigations. *J. Cryst. Growth* **2001**, *229*, 580–585.
31. Fujikawa, Y.; Sadowski, J.; Kelly, K.; Nakayama, K.; Mickelson, E.; Hauge, R.; Margrave, J.; Sakurai, T. Adsorption of Fluorinated C^{60} on the Si (111)-(7×7) Surface Studied by Scanning Tunneling Microscopy and High-Resolution Electron Energy Loss Spectroscopy. *Jpn. J. Appl. Phys* **2002**, *41*, 245–249.
32. Poon, S. W.; Chen, W.; Wee, A. T. S.; Tok, E. S. Growth Dynamics and Kinetics of Monolayer and Multilayer Graphene on a 6H-SiC(0001) Substrate. *Phys. Chem. Chem. Phys.* **2010**, *12*, 13522.
33. Rutter, G. M.; Crain, J. N.; Guisinger, N. P.; Li, T.; First, P. N.; Stroscio, J. A. Scattering and Interference in Epitaxial Graphene. *Science* **2007**, *317*, 219–222.
34. Simon, L.; Bena, C.; Vonau, F.; Aubel, D.; Nasrallah, H.; Habar, M.; Peruchetti, J. C. Symmetry of Standing Waves Generated By a Point Defect in Epitaxial Graphene. *Eur. Phys. J. B* **2009**, *69*, 351–355.
35. Jung, S.; Rutter, G.; Klimov, N.; Newell, D.; Calizo, I.; Hight-Walker, A.; Zhitenev, N.; Stroscio, J. Evolution of Microscopic Localization in Graphene in a Magnetic Field from Scattering Resonances to Quantum Dots. *Nat. Phys.* **2011**, *7*, 245–251.
36. Zhang, Y.; Brar, V.; Wang, F.; Girit, C.; Yayon, Y.; Panlasigui, M.; Zettl, A.; Crommie, M. Giant Phonon-Induced Conductance in Scanning Tunneling Spectroscopy of Gate-Tunable Graphene. *Nat. Phys.* **2008**, *4*, 627–630.
37. Efros, A.; Shklovskii, B. Coulomb Gap and Low Temperature Conductivity of Disordered Systems. *J. Phys. C: Solid State Phys.* **1975**, *8*, L49–L51.
38. Brar, V.; Zhang, Y.; Yayon, Y.; Ohta, T.; McChesney, J.; Bostwick, A.; Rotenberg, E.; Horn, K.; Crommie, M. Scanning Tunneling Spectroscopy of Inhomogeneous Electronic Structure in Monolayer and Bilayer Graphene on SiC. *Appl. Phys. Lett.* **2007**, *91*, 122102.
39. Premlal, B.; Cranney, M.; Vonau, F.; Aubel, D.; Casterman, D.; De Souza, M. M.; Simon, L. Surface Intercalation of Gold Underneath a Graphene Monolayer on SiC(0001) Studied

by Scanning Tunneling Microscopy and Spectroscopy. *Appl. Phys. Lett.* **2009**, *94*, 263115.
40. Choi, J.; Lee, H.; Kim, K. J.; Kim, B.; Kim, S. Chemical Doping of Epitaxial Graphene by Organic Free Radicals. *J. Phys. Chem. Lett.* **2010**, *1*, 505–509.
41. Choi, J.; Lee, H.; Kim, S. Atomic-Scale Investigation of Epitaxial Graphene Grown on 6H-SiC(0001) Using Scanning Tunneling Microscopy and Spectroscopy. *J. Phys. Chem. C* **2010**, *114*, 13344–13348.
42. Pereira, V.; Lopes dos Santos, J.; Castro Neto, A. Modeling Disorder in Graphene. *Phys. Rev. B* **2008**, *77*, 115109.
43. Hong, X.; Cheng, S. H.; Herding, C.; Zhu, J. Colossal Negative Magnetoresistance in Dilute Fluorinated Graphene. *Phys. Rev. B* **2011**, *83*, 085410.
44. Kelly, K.; Mickelson, E.; Hauge, R.; Margrave, J.; Halas, N. Nanoscale Imaging of Chemical Interactions: Fluorine on Graphite. *Proc. Natl. Acad. Sci. U. S. A.* **2000**, *97*, 10318–10321.
45. Johansson, L.; Owman, F. High-Resolution Core-Level Study of 6H-SiC (0001). *Phys. Rev. B* **1996**, *53*, 13793–13802.
46. Wong, S. L.; Huang, H.; Huang, Y. L.; Wang, Y. Z.; Gao, X. Y.; Suzuki, T.; Chen, W.; Wee, A. T. S. Effect of Fluorination on the Molecular Packing of Perfluoropentacene and Pentacene Ultrathin Films on Ag (111). *J. Phys. Chem. C* **2010**, *114*, 9356–9361.
47. Chen, W.; Wee, A. T. S. Synchrotron PES and NEXAFS Studies of Self-Assembled Aromatic Thiol Monolayers on Au(1 1 1). *J. Electron Spectrosc.* **2009**, *172*, 54–63.
48. Yu, X. J.; Wilhelmi, O.; Moser, H. O.; Vidyaraj, S. V.; Gao, X. Y.; Wee, A. T. S.; Nyunt, T.; Qian, H. J.; Zheng, H. W. New Soft X-ray Facility SINS for Surface and Nanoscale Science at SSLS. *J. Electron Spectrosc.* **2005**, *144*, 1031–1034.